Coating Fluoropolymer on BaTiO 3 Nanoparticles to Boost Permittivity and Energy Density of Polymer Nanocomposites

Xiu Liu, Fang-Yan Du, Junjin Che, Jia-Le Li, Ao-Shuang Yang, Jia-Hao Lv, Qiu-Yu Shen, Li He, Yin-Tao Li, Yuan-Lin Zhou, et al.

Coating fluoropolymer on $BaTiO_3$ nanoparticles to boost permittivity and energy density of polymer nanocomposites

Xiu Liu [a], Fang-Yan Du [a], Junjin Che [b], Jia-Le Li [a], Ao-Shuang Yang [c], Jia-Hao Lv [a], Qiu-Yu Shen [a], Li He [a], Yin-Tao Li [a], Yuan-Lin Zhou [a], Jinkai Yuan[b], Quan-Ping Zhang [a]*

[a] *State Key Laboratory of Environment-friendly Energy Materials, School of Materials Science and Engineering, Southwest University of Science and Technology, Mianyang 621010, China*
[b] *Centre de Recherche Paul Pascal, CNRS, University of Bordeaux, UMR5031, 33600 Pessac, France*
[c] *Sichuan College of Architectural Technology, Deyang, 618000, China*

ABSTRACT

Significantly enhanced dielectric constant and energy storage density positively facilitate miniaturing dielectric capacitors for various applications in electronics and electrical devices. In this work, a fluoropolymer is coated on $BaTiO_3$ (BT) nanoparticles to form a core-shell structure (BT@PF80), which is used as additional dipoles to enhance the dielectric constant and energy density of polymer nanocomposites. Characterizations with various techniques show uniform dispersion of nanoparticles and good compatibility of interfaces in polymer nanocomposites. Furthermore, the dielectric constant increases from 7.85 of neat polymer to 9.43 of the nanocomposites filled with BT@PF80 while the dielectric loss further decrease from 0.05 to 0.04 at 1 KHz. Besides, 7.79 J/cm^3 of energy density is achieved at the nanocomposites filled with BT@PF80, which is 2.65 times higher than that of the neat polymer. This work presents a simple and effective means to enhance dielectric constant and energy density, which tends to fertilize the fabrications of polymer dielectrics for electric energy storage.

Keywords: $BaTiO_3$, energy density, dielectric constant, polymer nanocomposites

Corresponding authors: Quan-Ping Zhang
E-mails: zhangqp@swust.edu.cn

Introduction:

Polymer dielectrics for electric energy storage are featured with good plasticity[1-7], high breakdown strength and light weight, which are widely used in various fields to meet the increasing requirements of electronics and electrical applications, such as optoelectronics, pulse systems[8-11]. The energy storage density (U_e) of dielectrics can be derived from the formula: $\boldsymbol{U_e = \int \mathbf{E}\,\mathbf{dD}}$, where E is the external electric field and D is the electric displacement. In the case of linear dielectrics, U_e can be calculated from the equation: $\boldsymbol{U_e = \frac{1}{2}\varepsilon_0\varepsilon_r E_b^2}$, where ε_0 is the vacuum dielectric constant, ε_r and E_b are the dielectric constant and breakdown strength of the dielectrics, respectively[12-13]. It is obvious that the energy storage density of dielectrics is directly determined by ε_r and E_b. Although commercial biaxially oriented polypropylene (BOPP) displays extremely high breakdown strength (~800KV/mm), a relatively low dielectric constant leads to unsatisfied energy storage density[14-17].

Many strategies have been proposed to enhance the energy storage density of polymers, such as incorporating dielectric nanoparticles [18-23] and designing sandwich structures[24-30]. It has been well demonstrated that blending dielectric nanoparticles (such as $BaTiO_3$[18, 20,], $SrTiO_3$[31], $Ba_{0.6}Sr_{0.4}TiO_3$[32], etc.) with polymers can realize a higher ε_r than neat polymer. It should be pointed out that high loading of dielectric nanoparticles in polymers are required to obtain a high enough ε_r for satisfying energy density. However, incorporating high-loading dielectric nanoparticles is likely to cause various defects in polymer nanocomposites, such as interface incompatibility, agglomeration, and even voids[33-38]. A mass of space charges is accumulated at incompatible interfaces or voids, leading to significant leakage currents. Furthermore, the local electric field around the nanoparticles is about several times higher than the applied electric field[38, 39]. The defects coupled with electric filed concentration inevitably cause a reduced breakdown strength of polymer nanocomposites that is much lower than that of neat polymers. Therefore, incorporating high-loading dielectric nanoparticles into polymers is still a great challenge to make compromises between dielectric constant and breakdown strength to achieve satisfied electric energy density

Alternatively, coating dielectric nanoparticles with organics or inorganics tends to achieve a high energy density of polymer nanocomposites. On the one hand, coating layers with the similar molecular structure with polymer matrices likely avoid the formation of defects in polymer nanocomposites, such as nonuniform dispersion of nanoparticles and poor compatibility of interfaces [40]. On the other hand, it is reported that core-shell structured nanoparticles also promote the breakdown strength of polymer nanocomposites. This is due to the fact that the presence of coated dielectric transition layer weakens the electric field distortion [41]. Obviously, incorporating core-shell nanoparticles plays critical role in promoting energy density of polymer nanocomposites. Particularly, a fluoropolymer coated high-*k* nanoparticles are expected to further promote polarizations with the additional dipoles in polymer nanocomposites. Therefore, it tends to enhance dielectric constant meanwhile achieve uniform dispersion of nanoparticles and good compatibility of interfaces for low dielectric loss and high breakdown strength.

In this paper, a fluorinated polysiloxane is synthesized via anionic polymerization, which is further coated on $BaTiO_3$ (BT) nanoparticles to form a core-shell structure (BT@PF) via thiol-ene click reaction [40, 42]. Enhanced dielectric constant of BT@PF/poly (vinylidene fluoride-hexafluoropropylene) (P(VDF-HFP)) nanocomposites are detected due to the additional dipole polarization of coating layer. Meanwhile, the fluoropolymer also facilitates uniform dispersion of BT nanoparticles and good compatibility of interfaces in polymer nanocomposites. Finally, 7.79 J/cm^3 of energy storage density is achieved at BT@PF80/P(VDF-HFP) nanocomposites, which is 2.65 times higher than the neat polymer.

Experimental

Materials

$BaTiO_3$ (BT) nanoparticles (HBT-010) were supplied by Shandong Sinocera Functional Material Company. (3-Mercaptopropyl) triethoxysilane (KH580) was

supplied by Shanghai Macklin Biochemical Co., Ltd. Tetramethylammonium hydroxide (TMAH) and 2, 2-Dimethoxy-2-phenylacetophenone (DMPA) were purchased from Shanghai Aladdin Bio-Chem Technology Co., Ltd. 2,4,6,8-Tetramethyl-2,4,6,8-Tetravinylcyclotetrasiloxane (V_4) and 1,3,5-Trimethyl-1,3,5-tris(3,3,3-trifluoropropyl)cyclotrisiloxane (D_3F) were purchased from Guangdong Weng Jiang Reagent Co., Ltd. Poly(vinylidenefluoride-co-hexafluoropropylene) powders (P(VDF-HFP), Kynar Flex 2801, 10 wt.% HFP) were supplied by Akema China Investment Co., Ltd. All the raw materials were used as received.

Sample Preparation

Figure 1 schematically illustrates the preparation process of BT@PF80/P(VDF-HFP) films. Three steps were carried out as follows: **Step 1**: Synthesis of fluoropolymer. D_3F and V_4 (mass ratio of 80:20) as the monomers, TMAH was used as the initiator to synthesize poly (methylvinylsiloxane-methyltrifluoropropylsiloxane) (named as PF80) via anionic ring-opening polymerization[36, 43]. **Step 2**: Fabrication of BT@PF80 Nanoparticles. Firstly, hydroxylated BT nanoparticles (BT-OH) were obtained by ultrasonically treating BT nanoparticles with H_2O_2 solution. Secondly, BT nanoparticles (BT-SH) were obtained by mixing BT-OH nanoparticles with KH580 and stirring at 30°C for 48 h under nitrogen atmosphere. Thirdly, PF80 and DMPA were dissolved in a mixture of toluene and DMF (volume ratio 1:1). Then BT-SH nanoparticles were added into the mixture and kept at 80°C for 1 h under nitrogen atmosphere. After that, the mixture was centrifuged for washing with ethanol repeatedly and dried in a vacuum oven at 60°C over 12 h. Finally, BT@PF80 core-shell structured nanoparticles were obtained. **Step 3**: Preparation of BT@PF80/P(VDF-HFP) films. After grinding and screening, 3g BT@PF80 nanoparticles were ultrasonically treated in DMF for 30 min. Then, 97 g P(VDF-HFP) was added into the mixture and vigorously stirred for 12 h. After that, the suspension was cast into film on a glass plate, and then dried in a vacuum oven at 105°C for 12 h to fully remove DMF. Afterward, the cast films were heated at 205°C for 10 minutes and then quenched in ice water immediately[36]. The quenched films were dried in a vacuum at 70°C for 12 h and peeled

from the glass substrates. The average thickness of the films is about 10 μm. Finally, P(VDF-HFP) films at fixed 3 wt% BT@PF80 nanoparticles were obtained, named as BT@PF80/P(VDF-HFP). Besides, BT-OH/P(VDF-HFP) films were also fabricated with the same route in order to highlight the roles of fluoropolymer in shell layer.

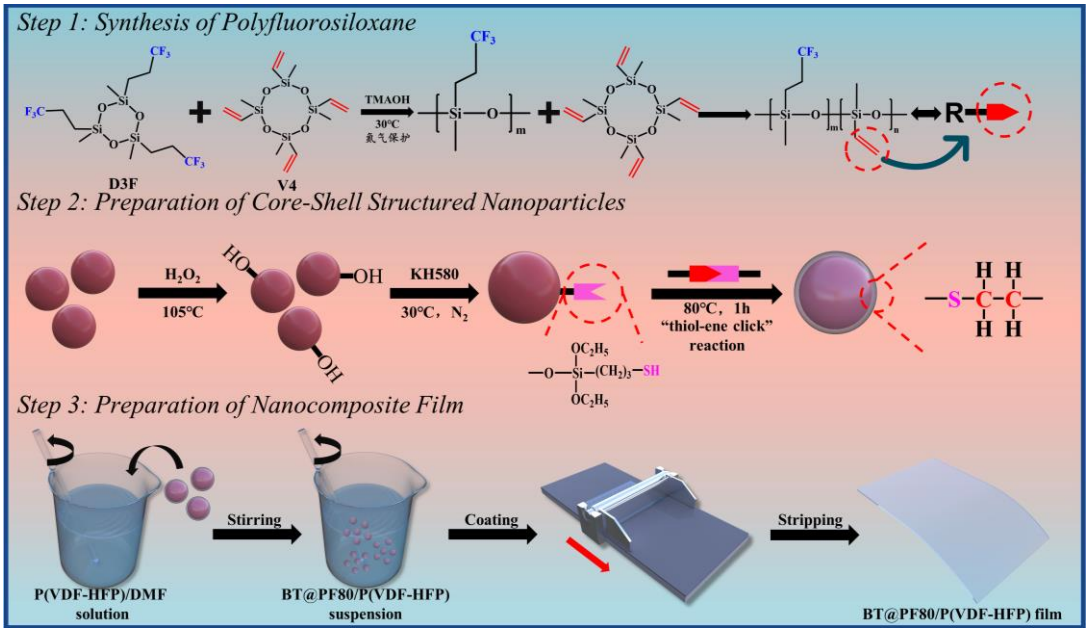

Figure 1. Schematic illustration of the preparation of BT@PF80/P(VDF-HFP) film.

Characterization

Superconducting nuclear magnetic resonance spectrometer (NMR, AVANCE Ⅲ 600MHz, Bruker, Swiss) and fourier transform infrared spectrometer (FT-IR, Nicolet iS50, Thermo Fisher Scientific, USA) were applied to characterize the structure of PF80. The morphology of BT@PF80 and various films were characterized by a scanning electron microscope (SEM, JSM-7610F, JEOL, Japan). In addition, transmission electron microscope (TEM, Tecnai G2 F20, FEI, USA) was used to examine the structure of BT@PF80. X-ray photoelectron spectrometer (XPS, ESCALAB Xi+, Thermo Fisher Scientific, USA) was used to test the surface chemical properties of BT@PF80. Thermogravimetric analysis (TGA, SDT Q600 V20.9 Build 20, TA, USA) was performed to measure the weight loss of BT nanoparticles with various treatments. X-ray diffraction (XRD, X'Pert PRO, Panaco, Netherlands) was applied to test the crystal structures of films. The dielectric properties of films were

evaluated at room temperature using Precision Impedance Analyzer (4294A, Agilent, USA). DC breakdown strength of films was tested using withstanding voltage tester (RK2672AM, Merrick, China). Polarization-electric field hysteresis loops (P-E loops) of films were performed at 100 Hz by a TF analyzer 3000 ferroelectric polarization tester (aixACCT Systems GmbH, Germany). Energy storage performance was calculated according to the *P-E* loops (Electrode area: 19.635 mm^2). Glass transition temperature (T_g) of films was detected by differential scanning calorimetry (DSC, NETZSCH 3500 Sirius) between 25°C and 200°C. Heating rate was fixed at 10°C/min under N_2 atmosphere.

Results and discussion

Figure 2 depicts FT-IR spectra and ^{1}H NMR spectra of PF80. As shown in **Figure 2(a)**, the absorption peaks at 3056 cm^{-1} (C-H stretching vibration), 1600 cm^{-1} (C=C stretching vibration) and 1408 cm^{-1} (C-H in-plane bending vibration) are corresponding to vinyl group. And the absorption peaks at 1445 cm^{-1} (C-H in-plane bending vibration), 1368 cm^{-1} (-CH_2-), 1316 cm^{-1} (CH_2-CH_2), 1211 cm^{-1} (-CF_3), and 901 cm^{-1} (C-CF_3) are attributed to trifluoropropyl group. Furthermore, the absorption peaks at 2965 cm^{-1} and 2907 cm^{-1} (C-H stretching vibration of -CH_3), 1265 cm^{-1} (Si-CH_3), 1150~1000 cm^{-1} (Si-O-Si stretching vibration), and 850~720 cm^{-1} (Si-C stretching vibration) are the methyl and the main chain of polysiloxane. The ^{1}H NMR spectra of PF80 in $CDCl_3$ provides more detailed evidence about the chemical structure, as shown in **Figure 2(b)**. The main H chemical shift peaks appear at δ=0.1-0.21 ppm, δ=0.73 ppm, δ=2.03 ppm, δ=5.80 ppm, δ=5.95 ppm, and δ=1.55 ppm, which are corresponding to the H chemical shifts of Si-CH_3(a), Si-CH_2-(b), -CH2CF_3(c), -CH=(d), CH=CH_2(e) and residual H_2O in PF80, respectively. To further determine the ratio of *m* to *n*, the intensity of b, c and e peaks are integrated. The chemical shifts integral area ratio of Peak b, Peak c and Peak e is approximately 1:1:0.3. Therefore, the fluorinated polysiloxane is a typical block copolymer and the block ratio of trifluoropropyl to vinyl is about 10:3. Therefore, FT-IR and ^{1}H NMR results show that a fluoropolymer with the vinyl group is successfully prepared.

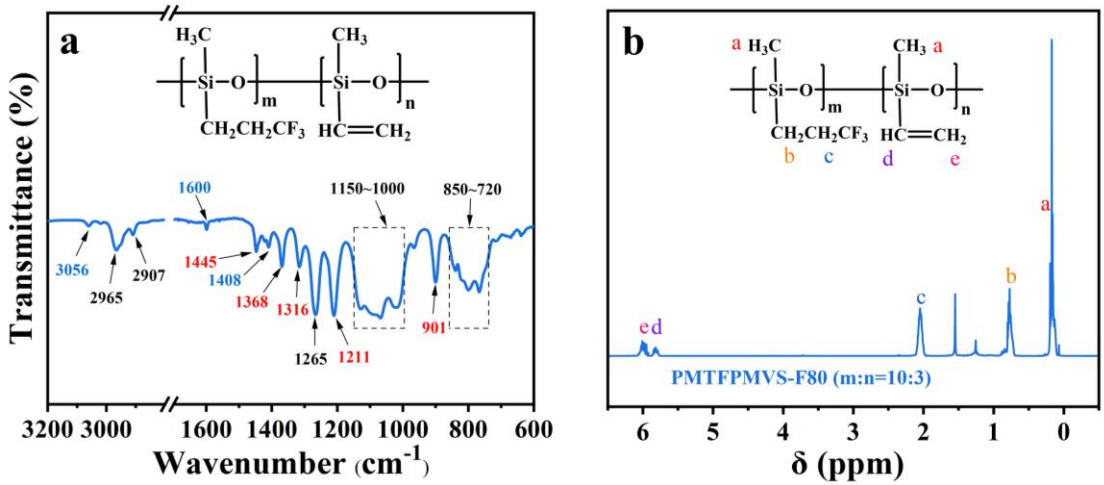

Figure 2. (a) FTIR spectra and (b) ^{1}H NMR spectra of the prepared PF80.

Figure 3 shows morphological observation results of BT@PF80 nanoparticles. BT nanoparticle is coated with a layer of substance, as shown in **Figure 3(a) and (b)**. And the thickness of the shell is about 2~3 nm, as shown in **Figure 3 (c)**. Furthermore, TEM-EDX mapping shows the elemental composition and distribution of BT@PF80 core-shell structured nanoparticles, as shown in **Figure 3(d)**. It is clear that Ba, Ti, O, Si, S and F are detected on the surfaces of BT@PF80. The contents of Ba, Ti and O elements are from BT nanoparticles. F and Si are mainly supplied by the side chains of PF80, and S is supplied by KH580. In addition, it can be found that S elements are mainly scattered among the core-shell structure region, indicating thiol groups of KH580 are successfully grafted onto the surface of BT nanoparticles (BT-SH). Meanwhile, the PF80 with vinyl group tends to react with BT-SH nanoparticles by classical thiol-ene click reaction, leading to uniform distribution of F around BT nanoparticles. The distribution of O, Si, S and F indicates that BT nanoparticles are coated with a relatively dense layer of PF80.

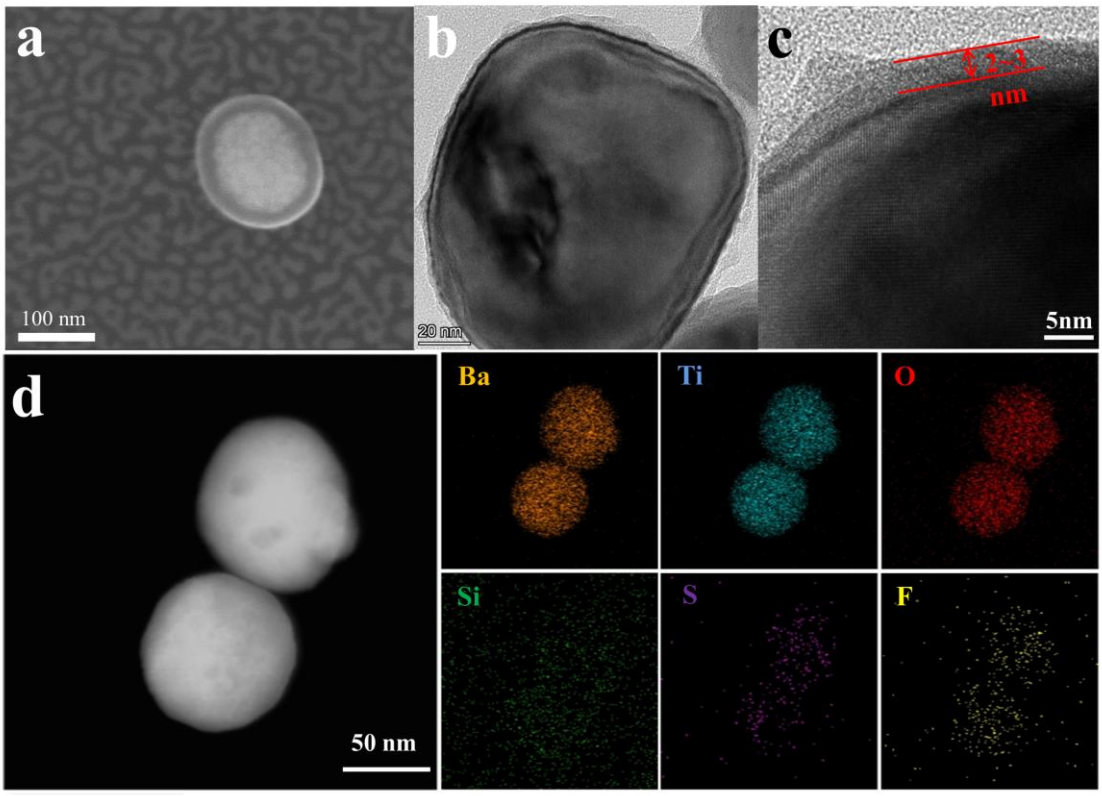

Figure 3. SEM images (a) and TEM images (b, c) and TEM-EDX mapping of BT@PF80 nanoparticles (d).

As shown in **Figure 4**, XPS technique is applied to further analyze the surface properties of BT@PF80 nanoparticles. In the wide-scan spectrum, strong signals of Ba, Ti, O and weak signals of Si, S can be detected. In the S2p spectrum, obvious peaks at 163.36 eV (S2p3/2) and 164.52 eV (S2p1/2) are detected because of the spin-orbit splitting of S2p, which is very close to the binding energy of S2p of mercaptan R-SH (164 eV). This is because the chemical environment around the S atom has changed after thiol-ene click reaction between BT-SH nanoparticles and PF80 with the vinyl group. It leads to the corresponding change of internal electron binding energy and the displacement of spectral peak. Furthermore, there is a strong peak at 102.05 eV in the Si2p spectrum, which is the binding energy of Si2p in PF80. Compared with the F1s spectrum of BT-SH, there is a weak peak at 688.5 eV in the F1s spectrum, which is the binding energy of F1s in PF80. The results further demonstrate that BT nanoparticles are coated with PF80.

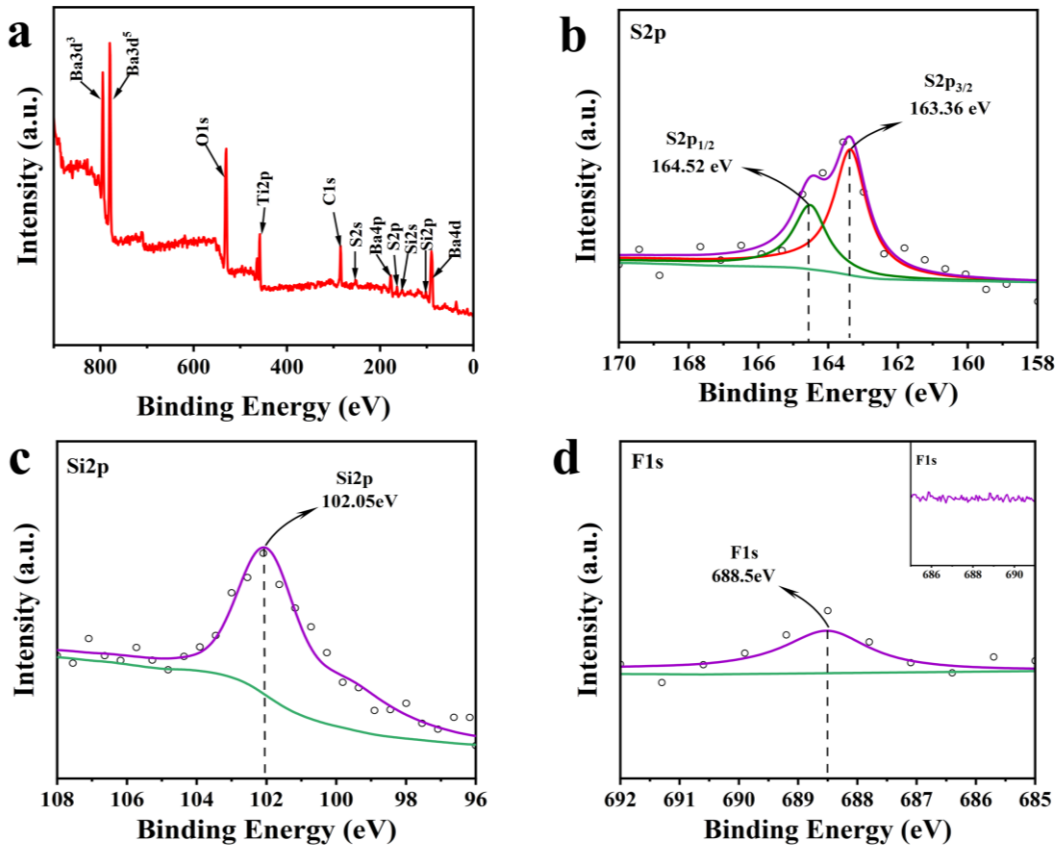

Figure 4. XPS results of BT@PF80, (a) wide-scan spectrum; (b) S2p spectrum; (c) Si2p spectrum; (d) F1s spectrum.

Figure 5 shows the morphology and structure of P(VDF-HFP) films. BT nanoparticles are uniformly distributed in BT@PF80/P(VDF-HFP) nanocomposite film, as shown in **Figure 5(a)**. However, obvious agglomerations of BT nanoparticles are observed in BT-OH/P(VDF-HFP) nanocomposite film, as shown in **Figure 5(b)**. It indicates that BT nanoparticles coated with PF80 promote the interaction with P(VDF-HFP) matrix, which lead to uniform dispersion of BT nanoparticles and good compatibility of the interfaces in the polymer nanocomposites.

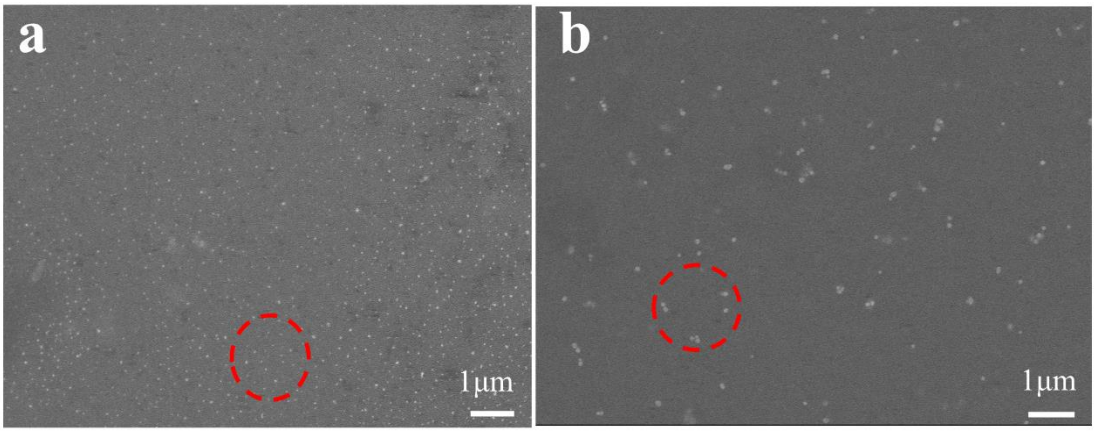

Figure 5. SEM image of (a) BT@PF80/P(VDF-HFP); (b) BT-OH/P(VDF-HFP).

To investigate the effects of functional fillers on the crystal structure of P(VDF-HFP), XRD, FT-IR, and DSC tests are conducted. XRD and FT-IR tests indicate that the crystal structures of P(VDF-HFP) remain unchanged after adding BT nanoparticles, as shown in **Figure S2a-b**. Besides, all P(VDF-HFP) based films exhibit α-phase after quenching. The α-phase has a lower residual polarization in comparison with β-phase, which is more favorable for electric energy storage [44]. From DSC results, it is clearly seen that the crystallinity of the film is slightly higher than the neat P(VDF-HFP) film, as shown in **Figure S3a-b**. This is due to the fact that BT nanoparticles act as heterogeneous nucleating agent. Importantly, the increase in crystallinity is beneficial for enhancing dielectric constant of polymer nanocomposites [22, 45].

Figure 6 shows the dielectric constant and dielectric loss of P(VDF-HFP) based films. Clearly shown is that BT@PF80/P(VDF-HFP) film displays the highest dielectric constants and neat P(VDF-HFP) exhibits the lowest values as a function of frequency among the films, and BT-OH/P(VDF-HFP) film in between, as shown in **Figure 6(a)**. It indicates that coating PF80 onto the surfaces of BT nanoparticles positively promotes dipole polarization. More importantly, BT@PF80/P(VDF-HFP) film shows the lowest dielectric loss as a function of frequency, as shown in **Figure 6(b)**. It further verifies that BT@PF80/P(VDF-HFP) film has good compatibility of the interfaces between BT@PF80 and P(VDF-HFP) that effectively inhibits the dielectric loss. To quantitatively determine the roles of PF80, the dielectric constant and dielectric

loss at 1k Hz are selected, as shown in **Figure 6(c)**. BT@PF80/P(VDF-HFP) film has about 9.43 of dielectric constant meanwhile about 0.04 of dielectric loss. Compared with neat P(VDF-HFP) film, 20.1% of the enhancement in dielectric constant are detected while its dielectric loss is suppressed from 0.05 to 0.04. The results demonstrate that BT nanoparticles coated with PF80 exert significant efforts on both dielectric constant and dielectric loss of BT@PF80/P(VDF-HFP) film.

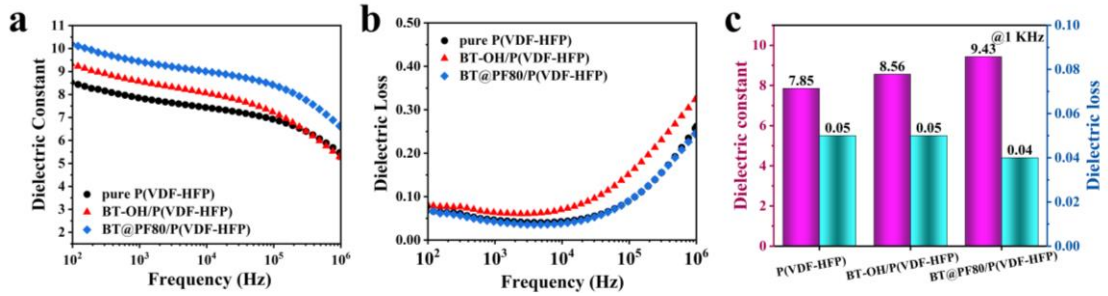

Figure 6. Dielectric constant and dielectric loss of P(VDF-HFP) based films, dielectric constant (a) and dielectric loss (b) as a function of frequency at room temperature. (c) Dielectric constant and dielectric loss at 1 k Hz.

Figure 7 depicts the electric polarization-electrical field (*P*-*E*) loops of P(VDF-HFP) based films at 10 Hz. The maximum polarizations (P_m) of P(VDF-HFP), BT-OH/P(VDF-HFP) and BT@PF80/P(VDF-HFP) films under 350 KV/mm is 3.11 μC/cm^2, 4.75 μC/cm^2, and 7.09 μC/cm^2, and the remnant polarizations (P_r) is 0.84 μC/cm^2, 1.29 μC/cm^2, and 1.44 μC/cm^2, respectively, as shown in **Figure 7(a)** to **(c)**. It is clear that P_m of BT@PF80/P(VDF-HFP) film is higher than the neat polymer. And BT-OH/P(VDF-HFP) films display only a slight increase in P_r, as shown in **Figure 7(d)**. The increased dipole polarization is mainly contributed by PF80 on BT nanoparticles.

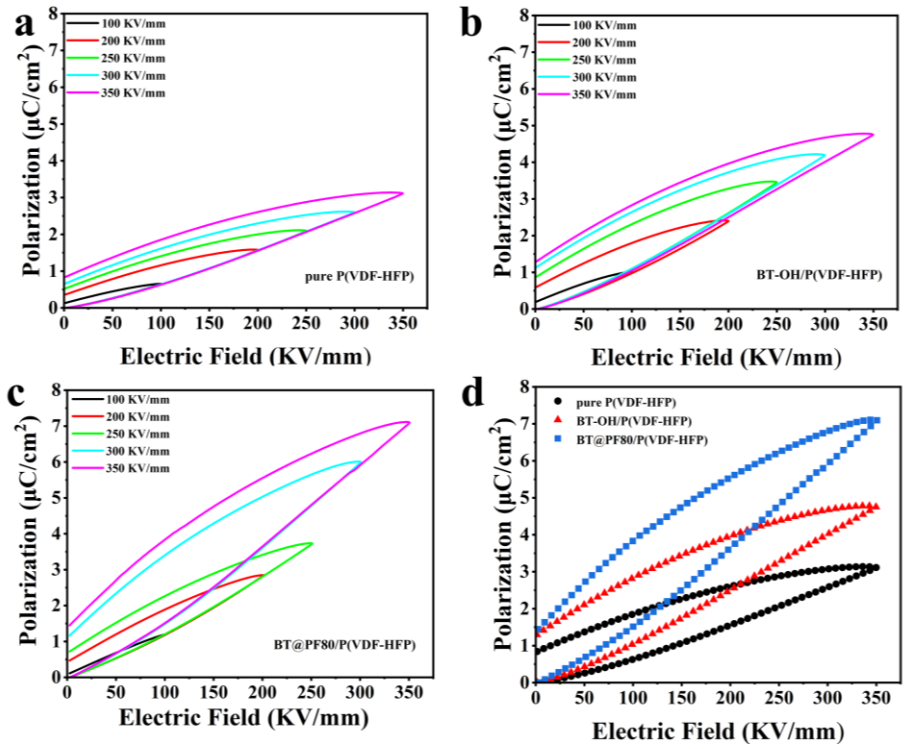

Figure 7. P-E loops of (a) neat P(VDF-HFP), (b) BT-OH/P(VDF-HFP) and (c) BT@PF80/P(VDF-HFP) films. (d) P-E loops of P(VDF-HFP) nanocomposite films at 350 KV/mm.

Breakdown strength is another important factor to electric energy storage density. The characteristic breakdown results of neat P(VDF-HFP) and its nanocomposite films are analyzed using Weibull statistics as follows:

$$p(E) = 1 - exp\left(-\left(E/E_b\right)^{\beta}\right)$$

where P(E) is the cumulative failure probability, E and E_b are the measured breakdown field and calculated breakdown field when the cumulative failure probability is 63.2%, and β is the shape parameter. Twelve points are selected for each sample to obtain E_b values while fitting with ln(-ln(1-P)). As shown in **Figure 8(a)**, BT@PF80/P(VDF-HFP) film shows 328 KV/mm of breakdown strength, which is inferior to BT-OH/P(VDF-HFP) and neat P(VDF-HFP) film. This is due to the fact that there is a coupling relationship on the dielectric constants of core layer, shell layer and polymer matrix [46, 47]. Although introducing the fluoropolymer on BT nanoparticles facilitates increasing dielectric constant and suppressing dielectric loss, local electric filed concentration long with the gradient of BT nanoparticles, the fluoropolymer and P(VDF-HFP) matrix

usually occurs, which is negative to high breakdown strength. The good coupling relationship needs to further explored by tailoring the fluorine content in the shell layer.

However, BT@PF80/P(VDF-HFP) film displays a maximum polarization (7.09 μC/cm^2) while neat polymer displays about 3.11 μC/cm^2 at 350 KV/mm, as shown in **Figure 8(b)**. The energy storage densities of various polymer films are calculated with the P-E loops, as shown in **Figure 8(c)**. Note that U_e of neat P(VDF-HFP), BT-OH/P(VDF-HFP) and BT@PF80/P(VDF-HFP) films are 2.94 J/cm^3, 4.47 J/cm^3 and 7.79 J/cm^3, respectively. Compared to pure P(VDF-HFP), 165% of the enhancement in energy storage density can be achieved at BT@PF80/P(VDF-HFP). Besides, BT@PF80/P(VDF-HFP) displays 57.45% of energy storage efficiency, which is higher than that of 48.60% for neat P(VDF-HFP) and 49.96% for BT-OH/P(VDF-HFP) films, as shown in **Figure 8(d)**. It relates to the reduced defects in BT@PF80/P(VDF-HFP), which in turn reduces conduction losses and then improves energy storage efficiency.

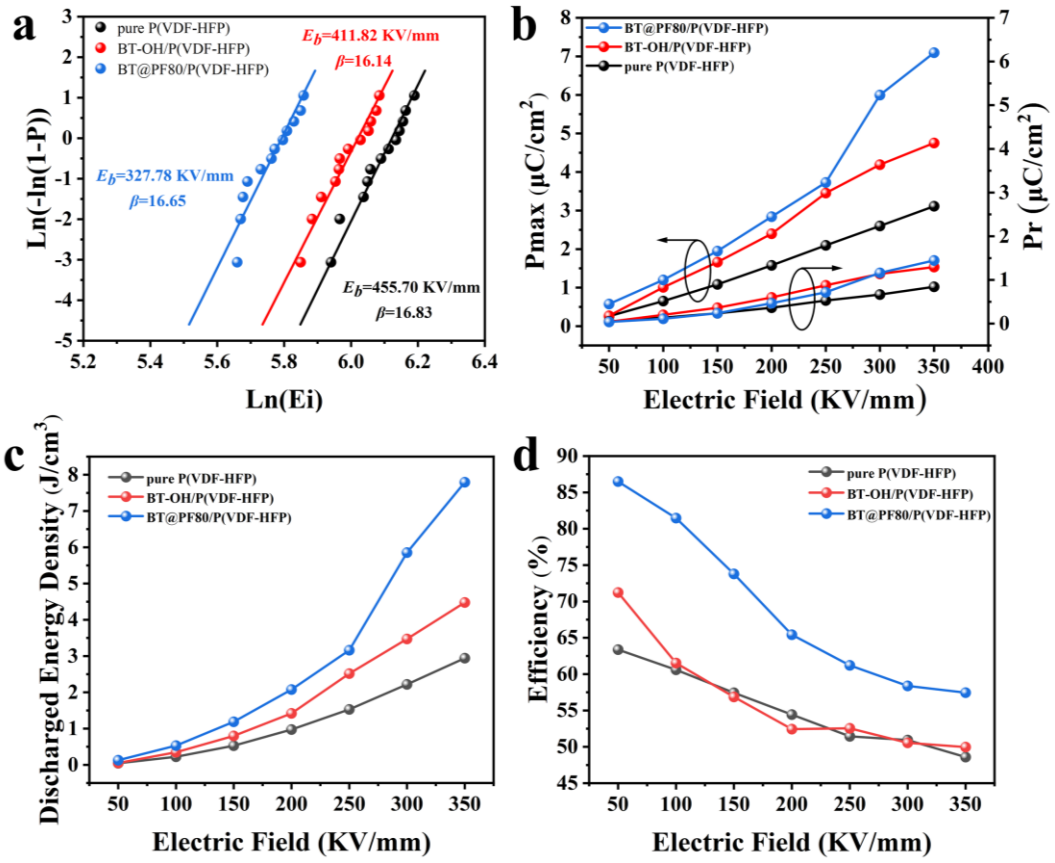

Figure 8. (a) Weibull distribution, (b)P_m & P_r, (c) discharge energy storage density and (d) energy storage efficiency of neat P(VDF-HFP), BT-OH/P(VDF-HFP) and BT@PF80/P(VDF-HFP) films

Conclusion

In conclusion, coating fluorinated polysiloxane on BT nanoparticles as a transition layer not only promotes the compatibility with P(VDF-HFP) matrix but also contributes dipole polarization in BT@PF80/P(VDF-HFP) film. It displays 9.43 of dielectric constant, which is 1.2 times to neat P(VDF-HFP) film. Meanwhile, it shows 0.04 of dielectric loss which is also lower than its counterpart. In addition, a 7.79 J/cm^3 of energy storage density is achieved at 350 KV/mm, which is 2.65 times to neat P(VDF-HFP) film. Besides, the energy storage efficiency increases from 48.60% to 57.45% of BT@PF80/P(VDF-HFP) film. This work presents a simple and effective method of dielectric gradient to enhance dielectric properties, which contributes to fertilizing the material designs for high electric energy storage.

Conflicts of interest

There are no conflicts to declare.

Acknowledgements

This work was supported by the National Natural Science Foundation of China (11747042), Natural Science Foundation of Sichuan Province (2022NSFSC0311) and Project of State Key Laboratory of Environment-friendly Energy Materials (21fksy16).

References

[1] S. Luo, J. Yu, S. Yu, R. Sun, L. Cao, W. H. Liao and C. P. Wong, *Adv. Energy Mater.*, 2019, 9, 1803204.
[2] Haque, Aman, Chen, Lei, Qi, Wang, Qing, Jackson, Tom and Long-Qing, *Nature*, 2015, 523, 576.
[3] Prateek, V. K. Thakur and R. K. Gupta, *Chem. Rev.*, 2016, 116, 4260.
[4] Xutong, Yang, Chaobo, Liang, Tengbo, Ma, Yongqiang, Guo, Jie and Kong, *Adv.*

Compos. Hybrid Mater., 2018, 1, 207.
[5] X. Hao, *J. Adv. Dielectr.*, 2013, 3, 1330001.
[6] H. Chen, V. V. Ginzburg, J. Yang, Y. Yang, W. Liu, Y. Huang, L. Du and B. Chen, *Prog. Polym. Sci.*, 2016, 59, 41.
[7] C. C. Han, X. H. Zhang, D. Chen, Y. H. Ma, C. W. Zhao and W. T. Yang, *J. Appl. Polym. Sci.*, 2020, 137, 12.
[8] Wang, Q., Zhu, L., *J. Polym. Sci., Part B: Polym. Phys.*, 2011, 49, 1421.
[9] M. Raquibuzzaman, B. Ray, T. B. Boykin and R. S. Gorur, *IEEE Trans. Dielectr. Electr. Insul.*, 2018, 25, 2375.
[10] S. A. Dibenedetto, A. Facchetti, M. A. Ratner and T. J. Marks, *Adv. Mater.*, 2009, 21, 1407.
[11] M. Mackey, A. Hiltner, E. Baer, L. Flandin, M. A. Wolak and J. S. Shirk, *J. Phys. D: Appl. Phys.*, 2009, 42, 175304.
[12] N. Guo, S. A. Dibenedetto, P. Tewari, M. T. Lanagan, M. A. Ratner and T., *J. Marks, Chem. Mater.*, 2015, 22, 1567.
[13] Z. Jiang, B. Xu, S. Prosandeev, J. Íñiguez, H. Xiang and L. Bellaiche, *Frontiers in Electronic Materials*, 2022, 2, 2673.
[14] H. Liu, B. X. Du and M. Xiao, *IEEE Trans. Dielectr. Electr. Insul.*, 2021, 28, 1539.
[15] D. M. Min, M. Z. Ji, Z. W. Gao, Z. L. Cai, Q. Z. Wu, J. Liu, S. T. Li and W. F. Liu, *J. Phys. D-Appl. Phys.*, 2022, 55, 12.
[16] D. Yue, Y. Feng, X. X. Liu, J. H. Yin, W. C. Zhang, H. Guo, B. Su and Q. Q. Lei, *Adv. Sci.*, 2022, 9, e2105773.
[17] Y. Feng, W. Tang, Y. Zhang, T. Zhang, Y. Shang, Q. Chi, Q. Chen and Q. Lei, *High Voltage*, 2021, 7, 242.
[18] L. Xie, X. Huang, Y. Huang, K. Yang and P. Jiang, *J. Phys. Chem. C*, 2013, 117, 22525.
[19] X. Zhang, *Adv. Mater.*, 2016, 28, 2055.
[20] M. S. Zheng, Y. T. Zheng, J. W. Zha, Y. Yang, P. Han, Y. Q. Wen and Z. M. Dang, *Nano Energy*, 2018, 48, 144.
[21] M. Guo, J. Jiang, Z. Shen, Y. Lin and Y. Shen, *Mater. Today*, 2019, 29, 49.
[22] Q. P. Zhang, W. F. Zhu, D. M. Liang, X. L. Wu, R. C. Chen, N. Sun, Y. T. Li and Y. L. Zhou, *Appl. Surf. Sci.*, 2019, 487, 77.
[23] J. Che, W. Neri, I. Ly, P. Poulin, C. Zakri and J. Yuan, *ACS Appl. Energy Mater.*, 2020, 3, 9107.
[24] C. Wang, G. He, S. Chen, D. Zhai, H. Luo and D. Zhang, *J. Mater. Chem. A*, 2021, 9, 8674.
[25] Q. Li, F. Liu, T. Yang, M. R. Gadinski and Q. Wang, *Proc. Natl. Acad. Sci. U. S. A.*, 2016, 113, 9995.
[26] F. Yan, X. He, H. Bai, B. Shen and J. Zhai, *J. Mater. Chem. A*, 2021, 9, 15827.
[27] C. Jie, Y. Wang, X. Xu, Q. Yuan, Y. Niu, Q. Wang and W. Hong, *J. Mater. Chem. A*, 2018, 6, 24367.
[28] Q. Sun, P. Mao, L. Zhang, J. Wang, Y. Zhao and F. Kang, *Ceram. Int.*, 2020, 46, 9990.
[29] Y. Shang, Y. Feng, C. Zhang, T. Zhang, Q. Lei and Q. Chi, *J. Mater. Chem. A*,

2022, 10, 15183.
[30] Y. Feng, J.-P. Xue, T.-D. Zhang, Q.-G. Chi, J.-L. Li, Q.-G. Chen, J.-J. Wang and L.-Q. Chen, *Energy Storage Mater.*, 2022, 44, 73.
[31] V. S. Nisa, S. Rajesh, K. P. Murali, V. Priyadarsini, S. N. Potty and R. Ratheesh, *Compos. Sci. Technol.*, 2008, 68, 106.
[32] T. Zhang, X. Zhao, C. Zhang, Y. Zhang and Q. Chen, *Chem. Eng. J.*, 2020, 408, 127314.
[33] X. Zhang, W. Chen, J. Wang, Y. Shen, L. Gu, Y. Lin and C. W. Nan, *Nanoscale*, 2014, 6701.
[34] P. Barber, S. Balasubramanian, Y. Anguchamy, S. Gong, A. Wibowo, H. Gao, H. Ploehn and H.-C. Zur Loye, *Materials*, 2009, 2, 1697.
[35] S. Zhang, C. Zou, D. I. Kushner, X. Zhou, R. J. Orchard, N. Zhang and Q. M. Zhang, *IEEE Trans. Dielectr. Electr. Insul.*, 2012, 19, 1158.
[36] F. Y. Du, R. C. Chen, J. Che, W. D. Xu, X. Liu, Y. T. Li, Y. L. Zhou, J. Yuan and Q. P. Zhang, *Phys. Chem. Chem. Phys.*, 2021,23, 26219.
[37] Q. Chi, T. Ma, Y. Zhang, Y. Cui, C. Zhang, J. Lin, X. Wang and Q. Lei, *J. Mater. Chem.* A, 2017, 5, 16757.
[38] S. L. Zhong, Z. M. Dang and J. W. Zha, *IEEE Trans. Dielectr. Electr. Insul.*, 2018, 25, 2122
[39] Z. M. Dang, J. K. Yuan, J. W. Zha, T. Zhou and G. H. Hu, *Prog. Mater Sci.*, 2011, 57, 660.
[40] R. C. Chen, Q. P. Zhang, K. Ke, N. Sun and W. Yang, *J. Mater. Chem. C*, 2020, 8, 8786.
[41] J. Ma, U. Azhar, C. Zong, Y. Zhang, A. Xu, C. Zhai, L. Zhang and S. Zhang, *Mater. Des.*, 2018, 164, 107556.
[42] Y. Ke, X. Huang, Z. Ming, L. Xie, T. Tanaka and P. Jiang, *ACS Appl. Mater. Interfaces*, 2014, 6, 1812.
[43] Q.-P. Zhang, J.-H. Liu, H.-D. Liu, F. Jia, Y.-L. Zhou and J. Zheng, *Appl. Phys. Lett.*, 2017, 111, 152901.
[44] L. Xie, X. Huang, C. Wu and P. Jiang, *J. Mater. Chem.*, 2011, 21, 5897.
[45] J. Li, Q. Meng, W. Li and Z. Zhang, J. *Appl. Polym. Sci.*, 2011, 122, 1659.
[46] J. W. Mcpherson, J. Kim, A. Shanware, H. Mogul and J. Rodriguez, *IEEE Trans. Electron Devices*, 2003, 50, 1771.
[47] Y. U. Wang, D. Q. Tan and J. Krahn, *J. Appl. Phys.*, 2011, 110, 044103.